



HAL
open science

Distribution and characteristics of Pleistocene ground thermal contraction polygons in Europe from satellite images

Pascal Bertran

► **To cite this version:**

Pascal Bertran. Distribution and characteristics of Pleistocene ground thermal contraction polygons in Europe from satellite images. *Permafrost and Periglacial Processes*, 2022, 33 (2), pp.99-113. 10.1002/ppp.2137 . hal-03691439

HAL Id: hal-03691439

<https://hal.science/hal-03691439>

Submitted on 9 Jun 2022

HAL is a multi-disciplinary open access archive for the deposit and dissemination of scientific research documents, whether they are published or not. The documents may come from teaching and research institutions in France or abroad, or from public or private research centers.

L'archive ouverte pluridisciplinaire **HAL**, est destinée au dépôt et à la diffusion de documents scientifiques de niveau recherche, publiés ou non, émanant des établissements d'enseignement et de recherche français ou étrangers, des laboratoires publics ou privés.

1 **Distribution and characteristics of Pleistocene ground thermal contraction polygons in Europe from** 2 **satellite images**

3 Pascal Bertran^{1,2}

4 ¹ Inrap, 140 avenue du Maréchal Leclerc, 33130 Bègles, France

5 ² PACEA, Université de Bordeaux – CNRS, allée Geoffroy-Saint-Hilaire, 33615 Pessac, France

6

7 **Abstract**

8 The study of Pleistocene polygons in Europe carried out using the collection of satellite images
9 available in Google Earth™ provides new data on the distribution of ground cracking by thermal
10 contraction during glacial periods and sheds light on some factors controlling their formation. The
11 distribution map shows that thermal contraction cracking affected terrain between latitude 43.5°N
12 and the southern limit of the Fennoscandian Ice Sheet at 15 ka, with a concentration of polygons
13 north of latitude 51°N. A clear asymmetry exists in relation to longitude, with a greater southward
14 extension of polygons in France (43.5°N) than in central Europe (47°N). Analysis of the characteristics
15 of polygons at the European scale reveals an association with lithology, latitude, and the age of the
16 sediments in which they formed. The morphological evolution over time reconstructed from
17 observations of polygons of contrasting ages indicates that a stable mature phase, characterized by
18 small (mean size 15 m), regular polygons with numerous Y-junctions, is reached after ca. 4 ka of
19 thermal contraction cracking activity.

20 **Keywords:** Ground thermal contraction polygons, Pleistocene permafrost, Europe

21

22 **1. Introduction**

23 The extent of past permafrost in Europe during the Last Glacial has been extensively studied in
24 recent decades based on the analysis of field data and palaeoclimatic simulations. Among the field
25 data, structures created by ground thermal contraction, including polygons remaining as cropmarks,
26 ice wedge pseudomorphs and relict sand wedges, have focused attention and their distribution was
27 used as a basis for evaluating the simulations ([Andrieux et al., 2016a](#); [Stadelmaier et al., 2021](#)).
28 Thermal contraction cracking occurs when the temperature of the frozen ground decreases rapidly
29 and causes severe stress exceeding the tensile strength of the ground. The cracks are filled by ice due
30 to the refreezing of water infiltrated from the surface (ice vein), by aeolian sands (sand vein) or close
31 in summer without significant infilling ([Mackay, 1975](#); [Mackay and Burn, 2002](#); [Murton, 2013](#)). In a
32 permafrost context, ice remains at depth and repeated cracking of the ground leads to the formation
33 of large ice wedges. When the permafrost thaws, the cavity created by ice melting is filled by the
34 collapse of the wedge walls and the former wedge shape is preserved as a pseudomorph. For a long
35 time, polygonal cropmarks, related to the differential growth of vegetation above the wedges and in
36 the center of polygons, have been interpreted as indicators of permafrost as they imply that wedges
37 have undergone sufficient growth to influence vegetation. [Andrieux et al. \(2016a\)](#) in the European
38 Pleistocene and [Wolfe et al. \(2018\)](#) in current Canadian Arctic, however, have shown that sand
39 wedges up to 1 m wide can form at the periphery of aeolian sand sources in areas of deep seasonal
40 frost (i.e., without permafrost) and are able to generate cropmarks. Polygons are therefore not

41 necessarily indicative of permafrost but of periglacial climates *sensu lato*. Polygons have also been
42 the subject of much work since similar structures have been recognized on planets other than Earth,
43 in particular Mars (e.g. [Mangold, 2005](#); [Ulrich et al., 2011](#)).

44 Satellite images accessible in Google Earth™ are a noteworthy data source for studying Pleistocene
45 thermal contraction polygons and have been widely used for this purpose in France by [Andrieux et al.](#)
46 [\(2016a,b\)](#). In particular, satellite images have an advantage over photos taken from airplanes as they
47 are easily accessible and usable in a geographic information system (GIS) and are free of distortion.
48 This paper proposes to extend the methodology used by [Andrieux et al. \(2016a\)](#) over entire Europe
49 to map polygon occurrences and characterize their morphology and size. This analysis is then
50 followed by comparison of the data with other layers of information, namely geographical location,
51 substrate lithology and age of the sediments in which they developed. The processing of a large
52 number of data located in various contexts gives hope that associations will appear more clearly
53 between the various parameters than in the framework of local studies, where variability is reduced.
54 After a brief review of literature, this paper presents the main results obtained on the distribution
55 and characteristics of Pleistocene thermal contraction polygons in Europe. Contribution to
56 permafrost mapping and to the evaluation of some factors involved in polygon formation is detailed.
57 This study can be used as a basis for further field studies to investigate thermal contraction cracks in
58 cross-section and to determine their nature and age.

59 **2. Background**

60 Ground thermal contraction polygons are remarkable figures in periglacial landscapes and, as such,
61 have prompted much work to determine their formation process and explain their morphological
62 variability. [Lachenbruch \(1962, 1966\)](#) laid the theoretical foundations for the mechanisms of soil
63 cracking by thermal contraction and the factors responsible for their organization into polygons. The
64 thermal stress to which a frozen soil is subjected leads to its fracturing. Cracks propagate
65 perpendicularly to the direction of the strongest stress. Repeated cooling events cause new cracks to
66 form in areas where stress has not been released by the opening of previous cracks. These cracks
67 typically have orthogonal (T-shaped) junctions. When the stress field is homogeneous and the stress
68 high relative to ground strength, the cracks are straight and generate regular orthogonal
69 (rectangular) polygons. When the stress is lower, local variations of ground strength cause the
70 deviation of the cracks that become sinuous and lead to the formation of irregular orthogonal
71 polygons. Homogeneous materials where strong stress can build up before cracking lead to
72 simultaneous crack initiation at distinct points and rapid crack propagation. This favors non-
73 orthogonal (Y-shaped) junctions leading to the development of hexagonal polygons.

74 Cracking is largely dependent on the linear coefficient of ground thermal expansion (which is variable
75 according to texture and ice content), thermal conductivity and strength (which is a function of
76 temperature). Particularly, fine-grained soils have a high coefficient and are, therefore, the most
77 prone to cracking. The progressive creation of new cracks causes the subdivision of polygons and
78 increases their regularity. Finally, the lateral heterogeneity of the stress field linked to the presence
79 of a water body and to slope can create orthogonal oriented polygons (i.e. polygons elongated along
80 a preferential direction).

81 Subsequent work has documented the conditions under which sufficient thermal stress occurs to
82 induce ground cracking in natural settings, identification of the factors driving variability in the

83 morphology of polygons, and description and simulation of their evolution over time. From sites in
84 Canada and Svalbard, [Fortier and Allard \(2005\)](#) and [Matsuoka et al. \(2018\)](#) showed that cracking
85 occurs when the surface ground temperature (T_s) drops below -20°C and the thermal gradient in the
86 first meter of ground (G) reaches $10^{\circ}\text{C}\cdot\text{m}^{-1}$. At some sites studied by [Matsuoka et al. \(2018\)](#), slightly
87 less drastic conditions ($T_s = -15^{\circ}\text{C}$, $G = 7^{\circ}\text{C}\cdot\text{m}^{-1}$) could locally be sufficient for crack initiation.

88 [Sletten et al. \(2003\)](#) in Antarctica, [Ulrich et al. \(2011\)](#) in the Canadian High Arctic, and [Haltigin et al.](#)
89 [\(2012\)](#) in Svalbard have analyzed the evolution of polygon morphology over time by studying
90 structures formed in sediments of various ages. These studies indicate that at the beginning,
91 polygons are large (20-50 m in diameter) and with mostly orthogonal junctions. With time, the
92 polygons subdivide and become smaller, more regular and non-orthogonal. According to [Sletten et](#)
93 [al. \(2003\)](#), evolution to a stable "mature" stage takes 10^4 to 10^6 years. [Haltigin et al. \(2012\)](#),
94 however, suggest that hexagonal polygons do not derive from the subdivision of initial orthogonal
95 polygons, but that the two types follow a parallel evolution. The predominance of T- or Y-junctions
96 would depend primarily on cracking conditions at the time of their initial formation. [Ulrich et al.](#)
97 [\(2011\)](#) observe variations along slopes in Svalbard, with orthogonal polygons dominating downslope
98 in gravelly sediments and smaller hexagonal polygons in silt upslope. For the authors, the
99 morphology of polygons would be mainly related to topography, probably due to the associated
100 variations in water content and ground thermal conductivity.

101 [Plug and Werner \(2001, 2002, 2008\)](#) simulated the formation and evolution of thermal contraction
102 polygons. Their results largely validate previous hypotheses, including that crack spacing (and thus
103 polygon size) decreases with time while the number of 4-way (X-) junctions increases relative to 3-
104 way (T- or Y-) junctions. Average crack spacing also increases nonlinearly with crack depth, but this
105 pattern tends to be obscured by the subdivision of polygons. Although orthogonal T- or X-junctions
106 are predominant, approximately equiangular (i.e. pseudo Y-shaped) 3-way junctions are formed
107 when a crack propagates towards the bend of a pre-existing crack ([Fig. 1](#)). This process occurs more
108 frequently as the heterogeneity of the ground increases, since crack sinuosity itself increases with
109 heterogeneity. These authors found that a steady state is reached relatively quickly, after 800
110 simulated years, which corresponds to a significantly longer time in natural settings, as thermal
111 contraction cracking does not necessarily occur every year (e.g. [Mackay and Burn, 2002](#); [Kokelj et al.,](#)
112 [2014](#)). They also showed that thermal contraction is sensitive to climatic extremes and weakly
113 related to average ground temperature.

114 Various regional, more rarely country-wide, studies of Pleistocene polygons visible as cropmarks in
115 Europe have been conducted by [Williams \(1964\)](#), [Gemmell and Ralston \(1965\)](#), [Svensson \(1973,](#)
116 [1988\)](#), [Christensen \(1974\)](#), [Johnsson \(1984\)](#), [Heyse and Ghysels \(2003\)](#), [Hassenpflug \(2013\)](#), [Andrieux](#)
117 [et al. \(2016a\)](#), [Ewertowski et al. \(2017\)](#), and [Beerten et al. \(2021\)](#), in addition to many reports of
118 isolated sites. These studies illustrate the distribution of lands affected by Pleistocene thermal
119 contraction and were used here as a starting point for a survey from satellite images. Among the
120 studies, only a few focused on investigating the associations between polygon size or morphology
121 and physical parameters, in particular ground lithology and topographic context. [Andrieux et al.](#)
122 [\(2016\)](#) in France concluded that there is no clear relationship between these parameters. [Beerten et](#)
123 [al. \(2021\)](#) in Belgium found that orthogonal polygons are preferentially found on valley borders while
124 polygons on higher surfaces are dominantly non-orthogonal.

125 3. Methods

126 Ground thermal contraction polygons were located from published data in the literature and from an
127 examination as exhaustive as possible of collections of satellite images accessible in Google Earth™,
128 following the method used for France by [Andrieux et al. \(2016a,b\)](#). Each site was named after the
129 nearest town or village and numbered from 1 to n in the case of multiple neighboring sites. For each
130 piece of land, a screenshot with a scale in meters was made and used as a basis, after contrast
131 adjustment, for measuring the size of polygons and for describing their main characteristics. The size
132 of polygons was measured where their visibility was sufficient according to the method proposed by
133 the same authors using ImageJ, an open-source image processing software (US National Institute of
134 Health, <http://imagej.nih.gov/ij/>), which allows for precise measurements. The number of cracks
135 (more exactly the surface expression of underlying wedges) intercepting three profiles drawn across
136 the polygon field was counted. The ends of each profile were set approximately at the center of a
137 polygon. Whenever possible, the profiles were arranged at a 60° angle to each other to average out
138 variations related to possible polygon elongation. The size of polygons corresponds to the total
139 length of profiles divided by the number of cracks, i.e. between 25 and 40 counted cracks in each
140 piece of land, with a few exceptions (for the largest polygons). The widths obtained in this way
141 (which do not correspond to true polygon diameters, as the profiles do not necessarily intersect all
142 polygons in their center) are comparable to the spacing of wedges such that it can be measured from
143 cross-sections. They are also similar to the values used in the simulations by [Plug and Werner \(2002\)](#).
144 The values are given in meters with one digit after the decimal point, although it is probably not
145 significant. Statistical comparison of size means calculated from polygon subsets was made using
146 PAST version 3.14 software ([Hammer et al., 2001](#)). The morphology of polygons was then classified
147 according to the criteria outlined by [Lachenbruch \(1966\)](#) and [Ewertowski et al. \(2017\)](#), which involve
148 the type of junction between cracks, the regularity of crack spacing, and the variability in crack width.

149 The coordinates of the polygon fields were used to generate a file using the GIS software QGIS
150 version 3.10. The references and date of the satellite images shown in Google Earth™ were recorded.
151 The altitude was determined using the EU-DEM with a horizontal resolution of 30 m
152 (<https://land.copernicus.eu/imagery-in-situ/eu-dem/eu-dem-v1.1/>). The ground lithology was
153 extracted from variable sources depending on the country. For France and the UK, the 1:50,000
154 digital geological map data (<http://infoterre.brgm.fr/> and [https://data.gov.uk/dataset/02af8783-
155 e3f6-4516-8efa-1e7059ddde26/bgs-geology-50k](https://data.gov.uk/dataset/02af8783-e3f6-4516-8efa-1e7059ddde26/bgs-geology-50k), respectively) were used. For Germany, the data are
156 from the 1:200,000 geological map (<https://services.bgr.de/wms/geologie/guek200/>), while for the
157 rest of Europe the data are from the 1:1,000,000 geological map ([http://onegeology-
159 geonetwork.brgm.fr/](http://onegeology-
158 geonetwork.brgm.fr/)). In Central Europe, these data have been supplemented for aeolian deposits
159 using the map proposed by [Lehmkuhl et al. \(2021\)](#). Some uncertainty remains in the precise
160 determination of lithology because of the scale of the geological maps and the difficulty of assessing
161 the thickness of the formations shown on these maps. Because of the large number of sites analyzed,
162 it is assumed that this uncertainty does not obscure the preferred association of polygons with
163 certain lithologies. Ice sheet limits at various times were taken from [Hughes et al. \(2016\)](#) for the
164 Fennoscandian Ice Sheet (FIS) and British-Irish Ice Sheet (BIIS), supplemented by data from [Evans et
165 al. \(2021\)](#), and [Ehlers and Gibbard \(2004\)](#) for the other ice sheets.

166 A total of 1311 polygon sites were identified. By nature, cropmarks are only identifiable in cultivated
167 plots, and forest and urbanized areas did not yield any data. The ability to distinguish cropmarks
168 depends largely on weather conditions and the stress under which the vegetation grows. Therefore,
169 the date of the satellite images and the nature of the crops play a major role. On a local scale, regions

170 devoid of polygons may result from inappropriate observation conditions rather than actual absence.
171 On a European scale, however, this issue has no real impact on the general distribution of terrains
172 affected by thermal contraction cracking. Many polygons (referred to as 'incomplete/limited' in [Table](#)
173 [S1](#)) are only visible in a limited area or are poorly distinct. Among the most legible polygons, 238
174 were measured and considered a representative set of the various lithological and latitudinal
175 contexts. The number of measured polygons from areas deglaciated at the very end of the Last
176 Glacial remains small, however, because of the limited extent of those areas compared to
177 unglaciated areas.

178 **4. Results**

179 **4.1. Distribution**

180 The main observations that can be made from the polygon distribution map ([Fig. 2](#)) are as follows:

181 (1) Polygons occur in a band approximately bounded to the south by latitude 44°N and to the north
182 by the ice sheet limit at 15 ka. Variations are visible according to longitude. In France, polygons exist
183 southward up to 44.5°N in Aquitaine and 43.5°N in the lower Rhone valley as already reported by
184 [Andrieux et al. \(2016a\)](#), whereas the southernmost polygons identified in central Europe (Hungary)
185 do not exceed 47°N. In addition, a few polygons can be observed in Sweden in areas deglaciated
186 between 14 and 15 ka at latitudes 56°N to 57°N, whereas no polygons have been identified in
187 Scotland at the same latitudes in areas deglaciated after 16 ka.

188 (2) Polygons are abundant north of latitude 51°N, in the UK, northern Belgium, the Netherlands,
189 northern Germany and Poland in various terrains. At lower latitudes, their distribution is reduced to
190 clusters. In these regions, the proximity of aeolian sand sources that provided the filling material for
191 thermal contraction cracks plays a decisive role. This factor was previously highlighted by [Andrieux et](#)
192 [al. \(2016a\)](#) in France south of latitude 48°N, where the occurrence of polygons is restricted to the
193 margins of coversands in Aquitaine, the Loire Valley ([Fig. 3A](#)), and the lower Rhone Valley. This also
194 holds true in central Germany on the left banks of the Main and Regnitz rivers, where polygons
195 developed in Keuper mudstones and sandstones at the periphery of aeolian sands ([Fig. 3B](#)), and in
196 Hungary on the right bank of the Raab River. In agreement, [Andrieux et al. \(2018\)](#) in France and
197 [Fabian et al. \(2013\)](#) in Hungary described relict sand wedges in cross-section in the same areas.

198 (3) Overall, the majority of the polygons are located in lowland, non-calcareous sedimentary terrain.
199 The main lithologies are, in order of decreasing abundance ([Fig. 4](#)), fluvial gravel, till, glaciofluvial and
200 aeolian sand, loess, and mudstone. The distribution is not homogeneous even in areas where
201 polygons are abundant, but areas of high spatial concentration appear. These are determined
202 primarily by a combination of favorable lithologies and a cover of appropriate satellite images. The
203 geologic maps used in this study tend to ascribe a predominantly glaciofluvial origin to the sands
204 outcropping in the Sand Belt at the periphery of the FIS, whereas other authors consider a large
205 proportion of these sands to be of aeolian origin ([Zeeberg, 1998](#); [Kasse, 2002](#); [Bertran et al., 2020](#)).
206 The relative proportion of the two types of substrate thus remains largely unknown.

207 (4) The influence of loess is variable. In Germany and Poland, many polygons are found in the
208 Northern European Loess Belt between latitudes 51°N and 52°N ([Fig. 2](#)). Conversely, no polygons
209 were identified in areas of thick loess cover in France and Belgium at latitude below 51°N. In these
210 areas, the ice-wedge pseudomorphs described in cross-sections (e.g. [Lautridou and Sommé, 1981](#);

211 [Frechen et al., 2001](#); [Deschodt et al., 2008](#); [Antoine et al., 2014](#)) predate the latest loess depositional
 212 phase and, because of the loess cover, do not generate cropmarks. This is probably also the case for
 213 the loess areas of central Germany ([Isarin et al., 1998](#)).

214 (5) Large lowland regions north of latitude 48°N are devoid of polygons, particularly in Eastern
 215 Europe (east of Poland, Slovakia). The factors behind are possibly the lack of suitable satellite cover
 216 and/or insufficient survey, as lithology and the extent of agricultural land do not seem to be involved.
 217 Despite the limitations, the data set is considered representative of the overall distribution of lands
 218 affected by polygon development.

219 **4.2. Polygon size**

220 Polygon sizes range from 3.7 m to 59.0 m, with a clear dependence on lithology although there is
 221 significant overlap between size ranges ([Fig. 5A](#)). The mean size in mudstones and tills is close to
 222 12 m with a lower limit of 4 m and an upper limit of 21 m (outliers excluded). Student's t-test
 223 ($p=0.561$) suggests that the hypothesis of similar means for both lithologies cannot be rejected. In
 224 sand and gravel, the mean size is 19 m, with a lower limit of 8 m. This mean is significantly different
 225 from that of mudstone and till ($p<0.001$). The largest polygons are found in sand and gravel, with
 226 many examples exceeding 30 m. Polygons in sandstone and loess are intermediate in size, with a
 227 mean close to 17 m. However, the Student's t test does not reject the hypothesis of similar means for
 228 sand, gravel, loess and sandstone at the 5% confidence level. The association with lithology
 229 essentially reflects the linear thermal expansion coefficient of the ground ([Lachenbruch, 1962](#)).
 230 Strong variability in size for a given lithology shows, however, that the thermal expansion coefficient
 231 alone cannot explain the size of polygons. Analysis of size as a function of the age of the sediments in
 232 which the polygons were formed also reveals a clear association ([Fig. 5B](#)). In Sweden, polygons from
 233 areas deglaciated after 15 ka are large (mean 28 m) ([Fig. 6](#)). As no polygons were observed in areas
 234 deglaciated after 14 ka, i.e. in the early Lateglacial, this suggests that thermal contraction, if active,
 235 only occurred for a few hundred years. Size decreases markedly for areas deglaciated after 17 ka
 236 (mean 22 m) and reaches in areas deglaciated after 19 ka, i.e. for ca. 4 ka of activity, a value
 237 comparable to that of areas that remained unglaciated (mean between 11 and 15 m depending on
 238 lithology). Because of the small number of polygons measured, t-test ($p=0.353$) does not reject the
 239 hypothesis of similar means between polygons < 15 ka and polygons < 17 ka. Similarly, polygons in
 240 the proglacial lakes Humber and Fenland (UK), which were drained after 16 ka ([Fairburn and](#)
 241 [Bateman, 2016](#); [Bateman et al., 2018](#); [Evans et al., 2018a](#)), are characterized by a very large size
 242 (mean 39 m).

243 Large polygons also exist locally in unglaciated areas, including sandy loess south of Wroclaw, Poland
 244 (latitude 51°N), sands in Turnhout, Belgium ([Beerten et al., 2021](#); latitude 51.3°N), and fluvial gravels
 245 near Oxford, UK (latitude 51.7°N). Without precise data on the age of host sediments and/or the
 246 infilling of cracks, the factor behind these large polygons cannot be determined.

247 Overall, there is only weak association of polygon size with latitude ([Fig. 5C](#)) and the average is
 248 between 14 and 20 m (mean 17.3 m) over the entire latitudinal range. The mean size increases
 249 slightly with latitude, however. Excluding the outliers (which may correspond to young polygons)
 250 from calculation results in more similar size means, which cannot be distinguished by statistics
 251 (except for the 55-57°N subset). The most striking change remains the larger size range at latitudes >
 252 49°N than at lower latitudes.

253 **4.3. Polygon morphology**

254 Following the nomenclature proposed by [Lachenbruch \(1966\)](#) and [Ewertowski et al. \(2017\)](#), polygon
255 morphology was classified according to the dominant junction type, the regularity of the pattern
256 created by polygons, and the homogeneity of wedge width.

257 Polygons can be hexagonal (predominance of Y-junctions), orthogonal (T- or +-junctions) or mixed
258 (coexistence of both types of junctions) ([Fig. 7](#)). In general, mixed polygons that combine both Y- and
259 T-junctions largely dominate ([Fig. 8A](#)). The lithology does not appear to have a clear influence on the
260 type of polygons, although orthogonal polygons are most abundant in tills ([Fig. 8B](#)). In contrast,
261 latitude plays a significant role, with orthogonal polygons predominating at high latitudes whereas
262 hexagonal polygons are mostly found in mid-latitudes ([Fig. 8D](#)). The influence of latitude may explain
263 why orthogonal polygons are more frequent in till, which was deposited in northern Europe by the
264 Pleistocene ice sheets. At the scale of a single piece of land, areas of orthogonal polygons are
265 sometimes juxtaposed with areas of hexagonal or mixed polygons ([Fig. 7C](#)). Therefore, it is clear that
266 in many cases the former did not derive from the latter as already indicated by [Halltigin et al. \(2012\)](#).
267 Few sites with oriented orthogonal polygons were identified, i.e., 7 out of 1311 (0.5 %) ([Fig. 7F](#)). All
268 formed on slopes and the direction of elongation changes laterally with slope. The relative elevation
269 of polygons to the surrounding terrain was quantified by calculating the average elevation within a
270 circular buffer of 1 km diameter centered on each site and subtracting this value from site elevation
271 (Δalt) ([Fig. 9](#)). Overall, the polygons are present on low relief terrain (mean $\Delta alt \sim 0$). Orthogonal
272 polygons tend to prevail in low-lying areas ($\Delta alt < 0$) that are likely poorly drained, while hexagonal
273 polygons are mostly located in elevated areas ($\Delta alt > 0$).

274 Wedges can be straight and regularly spaced, creating polygons of similar size and shape ('regular
275 polygons'). Conversely, wedges can be sinuous or wedge spacing can vary strongly ('irregular
276 polygons'). Irregular polygons dominate at high latitudes ([Fig. 8E](#)) and are on average larger than
277 regular polygons ([Fig. 8C](#)). In particular, large polygons formed in areas deglaciated at the very end of
278 the Pleniglacial in Sweden are all irregular and characterized by cracks that are often discontinuous
279 and of variable spacing ([Fig. 10](#)). In contrast, small regular polygons are most abundant in areas that
280 remained unglaciated, especially in mid-latitudes.

281 In some cases, the wedges are approximately of similar width, while in other cases noticeable
282 variations are visible ([Fig. 11](#)). The widest wedges generate a large network and are considered the
283 first cracks to have appeared (primary cracks) ([Lachenbruch, 1966](#)). A network of narrower secondary
284 wedges subdivides the large polygons. This category of polygons is referred to as 'subdivided'. A
285 gradation can be observed between large irregular subdivided polygons and small regular polygons
286 (< 15 m) with no identifiable hierarchy in wedge width. The latter appear to derive from the former
287 due to the growth of secondary wedges. For the majority of the subdivided orthogonal polygons,
288 secondary wedges form a net typified by more abundant Y-junctions than for primary wedges. At
289 some sites, areas of large simple polygons are juxtaposed with areas of subdivided polygons in
290 connection with variations of topography ([Fig. 11](#)). It seems that this results primarily from erosion,
291 with the shallowest secondary wedges disappearing more rapidly than primary wedges. This factor,
292 as well as the low potential of the narrowest wedges to create visible cropmarks, probably explains
293 to a large extent the coexistence of subdivided polygons and simple polygons in the same area and
294 on the same lithology. Subdivided polygons are present throughout the study area, except for the
295 sectors deglaciated after 17 ka (Sweden).

296 The proportion of 3-way (T or Y) and 4-way (X) junctions was counted on a sample of polygons of
297 contrasting ages. Comparison of the results obtained for young polygons, from areas deglaciated
298 after 15 ka and 17 ka respectively, shows that the proportion of 4-way junctions increases with time
299 in agreement with literature data (Plug and Werner, 2002) (Fig. 12A). In contrast, for longer periods
300 of thermal contraction activity (areas deglaciated after 22 ka and unglaciated areas), an opposite
301 trend is observed. This reflects the subdivision of polygons and the formation of secondary wedges
302 with dominant Y-junctions as indicated above. The diagram proportion of 4-way junctions as a
303 function of lithology (Fig. 12B) does not show a clear relationship between the two parameters but a
304 large variability in the proportion of 4-way junctions for each lithology. Loess appears to be an
305 exception with a low average proportion, reflecting a dominantly hexagonal morphology. However,
306 the sample of loess polygons analyzed is limited (N = 6) and probably not representative. Indeed,
307 Figure 8 shows that hexagonal polygons are in equivalent proportion in loess and other lithologies.

308 The nature of wedge fill when it could be determined from cross-sections does not seem to influence
309 polygon morphology. Similar polygons may correspond to a network of ice-wedge pseudomorphs or
310 relict sand wedges. Nevertheless, a few examples characterized by unusually wide wedges are
311 specifically associated with ice-wedge pseudomorphs. This is the case at Great Milton, UK (Fig. 11A),
312 where the wedges reach ca. 8 m width and are located near quarries showing large pseudomorphs
313 (Seddon and Holyoak, 1985; Maddy et al., 1998). Another example is Posthof_2 in Germany where
314 the wedges reach 5.5 m width and pseudomorphs have been reported nearby (Isarin et al., 1998).

315 5. Discussion

316 Overall, the distribution of polygons coincides with that of ice-wedge pseudomorphs and relict sand
317 wedges described in the literature (e.g. Watson, 1965; Michel, 1969, 1975; Svensson, 1973, 1988;
318 Haesaerts and Van Vliet-Lanoë, 1973; Christensen, 1974; Vandenberghe and Krook, 1981; Johnsson,
319 1984; Seddon and Holyoak, 1985; Gozdzik, 1986; Kolstrup, 1986, 2004; Brandon and Sumbler, 1991;
320 Isarin et al, 1998; Maddy et al., 1998; Antoine et al, 2005; Ghysels and Heyse, 2006; Kovács et al.,
321 2007; Ewertowski, 2009; Antoine et al., 2014; Buylaert et al., 2009; Jary, 2009; Fabian et al., 2013;
322 Worsley, 2014; Murton et al., 2015; Ruzkiczay-Rüdiger and Kern, 2016; Andrieux et al, 2016a;
323 Ewertowski et al., 2017; Evans et al., 2018b; Grube, 2021), although in detail many areas where
324 wedges were observed in cross-section are not associated with cropmarks (Fig. 13). This distribution
325 helps delineate the area that was affected by permafrost or deep seasonal frost during the
326 Pleistocene, in a context that was cold enough to allow repeated cracking of the ground by thermal
327 contraction. As the age of polygons in unglaciated areas and the duration of their development
328 remains unknown in most cases, uncertainty remains as to whether the observed distribution
329 reflects that of the Last Glacial or whether polygons formed during earlier glacials contributed
330 substantially.

331 The abundance of polygons in a band north of latitude 51°N suggests that thermal contraction
332 leading to the growth of large ice- or sand wedges was active until 18-17 ka, particularly in the North
333 European Loess Belt where loess deposition was still significant at that time (Meszner et al., 2013;
334 Schmidt et al., 2021). Many ice-wedge pseudomorphs have been described in the loess (Isarin et al.,
335 1998; Jary, 2009; Meszner et al., 2010), whereas sand wedges or composite-wedge pseudomorphs
336 dominate in the Sand Belt at the periphery of the FIS (Gozdzik, 1986; Buylaert et al., 2009;
337 Ewertowski, 2009; Grube, 2021). Further south, the lack of cropmarks in loess, particularly in France,
338 indicates that the growth of large wedges did not affect the later phases of loess deposition. This is in

339 agreement with stratigraphic observations and numerical ages obtained on ice-wedge
340 pseudomorphs, which show that the majority developed between 31 and 24 ka, during the period
341 referred to as Last Permafrost Maximum (LPM, [Vandenberghé et al., 2014](#); [Bertran et al., 2014](#)).

342 On the FIS margins, the distribution of polygons suggests that thermal contraction associated with
343 the growth of large ice- or sand wedges was not active in the areas deglaciated after 14 ka, i.e. during
344 the Lateglacial. This finding is contrary to the hypothesis widely discussed in the literature of wedge
345 development in northern Europe during the Younger Dryas (e.g. [Gemmel and Ralston, 1965](#);
346 [Svensson, 1988](#); [Isarin et al., 1998](#); [Evans et al., 2018b](#)). Currently, few OSL ages obtained on sand fills
347 are conclusive. In southern Sweden, a single OSL age indicates Weichselian Late Pleniglacial filling
348 ([Kjaer et al., 2006](#)). In Poland, all conventional OSL ages also point to the Late Pleniglacial
349 ([Ewertowski et al., 2017](#)). In France, however, [Andrieux et al. \(2018\)](#) using Single Grain OSL dating
350 have documented the formation of sand veins in already existing sand wedges, confirming the
351 existence of thermal contraction (associated with deflation) during the Younger Dryas. However, this
352 period alone did not lead to the creation of large wedges and cropmarks in France.

353 Overall, the distribution of polygons shows a clear east-west asymmetry, with the southern limit of
354 polygons reaching 43.5°N in France while it does not exceed 47°N in Hungary. This limit coincides
355 with that of the relict sand wedges described in cross-sections and the observed difference cannot be
356 attributed, therefore, to the lack of suitable satellite images. The main factor potentially involved in
357 this pattern could be the insulation of the ground by snow and/or vegetation, which reduced the
358 temperature gradient in the upper ground layer and limited thermal stress. Palaeoclimatic
359 simulations (e.g. [Stadelmaier et al., 2021](#)) suggest that the mean depth of winter snow cover during
360 the LGM (~21 ka) increased eastward from less than 10 cm on average in France to more than 50 cm
361 in Hungary. In France, the southernmost relict sand wedges are mainly located in areas of active
362 deflation (Aquitaine, lower Rhone Valley) where snow must have been blown away by the wind, as
363 attested by numerous field evidence (ventifacts, yardangs, aeolian pans) ([Sitzia et al., 2015](#); [Bosq et al., 2018](#)).
364 At the same time, simulations ([Strandberg et al., 2011](#); [Janská et al., 2017](#)) as well as
365 reconstructions based on pollen records ([Magyari et al., 2014](#)) also show that the vegetation cover
366 was denser and more shrubby in Eastern Europe than at the same latitude in Western Europe, thus
367 contributing to soil insulation.

368 In the southern fringe of the polygon extent, the distribution is restricted to areas at the periphery of
369 coversands, indicating that wedge growth was primarily due to sand infiltration into the cracks. In
370 France, the lack of ice-wedge pseudomorphs in adjacent terrain strongly suggests that thermal
371 contraction occurred in a deep seasonal frost context ([Andrieux et al., 2016a](#); [Stadelmaier et al., 2021](#)).
372 In Hungary, the periglacial structures mentioned in the literature are still few and do not allow
373 a clear statement on the presence or absence of permafrost. Nevertheless, palaeoclimatic
374 simulations suggest that the case of Hungary is similar to that of southwestern France (deep seasonal
375 frost). In central Germany, the same simulations indicate that the sand wedges developed in a
376 discontinuous permafrost context. Ground cracking would have been limited to areas where snow
377 deflation, associated with sand transport, was active.

378 Analysis of the characteristics of polygons at the European scale reveals an association with lithology,
379 latitude, and sediment age that could not be identified in regional analyses ([Andrieux et al., 2016a](#);
380 [Ewertowski et al., 2017](#); [Beerten et al., 2021](#)). Particularly, the average size of polygons is smaller on
381 fine-grained sediments and, therefore, in association with higher linear thermal expansion

382 coefficient, in agreement with the model of [Lachenbruch \(1966\)](#). Contrary to the assumption that
383 crack spacing increases with crack depth ([Plug and Werner, 2002](#)) and, therefore, with colder
384 climates, no clear association of polygon size with latitude appears when outliers are excluded from
385 calculation, probably because of the subdivision of polygons over time. Increased size range at high
386 latitudes may reflect greater variability in the age of host sediments, because of widespread
387 deposition of variable sediments (glaciofluvial sand, aeolian sand, loess) during the Weichselian Late
388 Pleniglacial.

389 This study also shows that orthogonal polygons, sometimes extremely regular (rectangular), are
390 mainly located in high latitudes ($>50^{\circ}\text{N}$), in areas that were not glaciated or were deglaciated before
391 17 ka. Such a distribution could reflect the role of climate. In agreement with [Lachenbruch \(1966\)](#),
392 the stress generated by very cold temperatures and a high temperature gradient in the subsurface
393 ground layer would be much greater than ground strength and would result in straight-line crack
394 propagation. Topography could also have played a role, orthogonal polygons being located in
395 depressions where ice could form in abundance in soils, whereas hexagonal polygons are located on
396 well-drained reliefs.

397 The duration of thermal contraction activity is also a key parameter for the size and regularity of
398 polygons. A long duration causes the subdivision of polygons that become small and regular, as
399 already indicated by the majority of authors (e.g. [Lachenbruch, 1966](#); [Sletten et al., 2003](#); [Ulrich et
400 al., 2011](#)). It helps explain a large part of the variability observed in Europe. Observations made on
401 series of polygons of contrasting ages allow us to propose an evolutionary sequence, whose main
402 steps are as follows:

403 (1) After a few hundred years of activity, thermal contraction cracks give rise to large (typically 30 m)
404 and irregular (cracks with variable spacing), poorly formed polygons.

405 (2) After about 2 ka, the number of cracks and their continuity increases while the size of the
406 polygons decreases significantly (typically 22 m). Regular orthogonal (rectangular) polygons develop
407 in very cold areas at high latitudes, whereas irregular polygons form preferably in less cold regions
408 due to increased crack sinuosity.

409 (3) After about 4 ka, the polygons are well developed and their size becomes comparable to that of
410 polygons in areas exposed for a long time to thermal contraction. This size is of the order of 15 m for
411 all lithologies combined. The polygons become subdivided; primary cracks widen and contrast with
412 narrow secondary cracks. The latter have Y-junctions in greater proportion than primary cracks,
413 possibly because of greater homogeneity of the ground on a small scale than on a field-wide scale.

414 (4) In the longer term, the difference in width between primary and secondary cracks diminishes due
415 to the growth of ice- or sand wedges. The polygons form a regular pattern in which Y-junctions are in
416 high proportion (hexagonal or mixed polygons). Dominant Y-junctions may result from intensive
417 subdivision and from the evolution of orthogonal 3-way junctions formed in crack bends into Y like
418 junctions ([Fig. 1B](#)). The size stabilizes around 15 m on average. It is possible that the speed with
419 which this maturity phase is reached is variable depending on the nature of the wedge filling. Ice has
420 a significantly lower strength than frozen sand and the surrounding sediments. Preferential cracking
421 of ice leads to rapid wedge growth (e.g. [Plug and Werner, 2002](#)). This factor, combined with the
422 collapse of the walls during ice melting, probably accounts for the formation of polygons with wide
423 primary wedges contrasting with narrow secondary wedges. The contrast in strength between the

424 host sediment and the sandy fill is smaller, so that subdivision likely progresses more rapidly,
425 favoring the evolution towards a stable mature phase. According to [Burn and O'Neill \(2015\)](#), the
426 location of polygons in the landscape (i.e. in depressions or on hillslopes) may also affect the speed
427 of subdivision and secondary ice-wedge growth.

428 In unglaciated areas, the age of polygons and the duration of development remains unknown in most
429 cases. Available stratigraphic data and ages obtained on the infill and host sediments suggest that
430 ground thermal contraction cracking must have been repeatedly active during the Last Glacial (e.g.,
431 [Vandenberghe and Krook, 1981](#); [Buylaert et al., 2009](#); [Worsley, 2014](#); [Andrieux et al., 2018](#)) and,
432 therefore, may correspond to several millennia of cumulated evolution. In some cases, there is
433 evidence of activity spanning the Mid- to Late Pleistocene (e.g., [Andrieux et al., 2018](#)). Extensive
434 dating would be necessary to better evaluate this point.

435 **6. Conclusions**

436 The study of Pleistocene polygons in Europe carried out using the collection of satellite images
437 available in Google Earth™ provides new data on the distribution of ground cracking by thermal
438 contraction during glacial periods and sheds light on some factors controlling their formation.
439 Overall, the distribution map indicates that this process affected terrain between latitude 43.5°N and
440 the southern limit of the FIS at 15 ka, with a concentration of polygons north of latitude 51°N. A clear
441 asymmetry is visible in relation to longitude, with a greater southward extension of polygons in
442 France (43.5°N) than in central Europe (47°N), potentially related to thicker snow cover and denser
443 vegetation towards the east insulating the ground from temperature variations. In the southern
444 fringe of the polygon extent, these are mainly present in areas at the margin of aeolian sands. In
445 these areas, sand wedges were formed in a context of deep seasonal frost (France and probably
446 Hungary) or possibly of discontinuous permafrost (central Germany). Further investigations in the
447 latter region would be necessary to investigate this in more details.

448 The morphological evolution over time reconstructed from observations of polygons of contrasting
449 ages in Europe broadly confirms that already described in current periglacial environments. The
450 stable mature phase, characterized by small (average size 15 m), regular polygons with numerous Y-
451 junctions, seems to be reached after ca. 4 ka, faster than previously mentioned. Further field
452 investigations to document wedge morphology as well as the nature and age of their infill should
453 allow for a better characterization of the glacial environments and the mapping of the Pleistocene
454 permafrost.

455 **Acknowledgements**

456 I thank J.P. Coutard, F. Didierjean, B. Douteyssier, C. Ferrier, J.M. Marion, S. Meszner and M. Rué for
457 providing me with aerial photographs of polygons. I am also indebted to E. Andrieux, with whom this
458 study was initiated for French polygons. J. Murton, J. Vandenberghe and an anonymous reviewer are
459 greatly acknowledged for their thorough review of the manuscript and interesting comments.

460 **Supplementary information**

461 Table S1: List of polygon sites identified from satellite images with their location and indication of
462 elevation (alti_DEM, in m a.s.l. rounded to the nearest integer), lithology and size (in m) measured
463 from the images. French polygons are taken from [Andrieux et al. \(2016b\)](#), with some additions. When
464 available, the geological codes are taken from the geological maps listed in the main text.

465 **Declaration of competing interest**

466

467 The author declares that he has no known competing financial interests or personal relationships
468 that could have appeared to influence the work reported in this paper.

469

470 **References**

471 Andrieux E., Bateman M., Bertran P., 2018. The chronology of Late Pleistocene thermal contraction
472 cracking derived from sand wedge dating in central and southern France. *Global Planetary Change* 162,
473 84-100.

474 Andrieux E., Bertran P., Saito K., 2016a. Spatial analysis of the French Pleistocene permafrost by a GIS
475 database. *Permafrost and Periglacial Processes* 27, 17-30.

476 Andrieux E., Bertran P., Antoine P., Deschodt L., Lenoble A., Coutard S. & collaborators, 2016b.
477 Database of Pleistocene periglacial features in France: description of the online version. *Quaternaire*
478 27 (4), 329-339.

479 Antoine P., Marchiol A., Brocandel M., Gros Y., 2005. Découverte de structures périglaciaires (sand-
480 wedges et composite-wedges) sur le site de stockage de déchets radioactifs de l'Aube (France).
481 *Comptes Rendus Géosciences* 337 (16), 1462-1473.

482 Bateman M.D., Evans D.J.A., Roberts D.H., Medialdea A., Ely J., Clark C.D., 2018. The timing and
483 consequences of the blockage of the Humber Gap by the last British-Irish Ice Sheet. *Boreas* 47, 41-61.

484 Beerten K., Meylemans E., Kasse C., Mestdagh T., Van Rooij D., Bastiaens J., 2021. Networks of
485 unusually large fossil periglacial polygons, Campine area, northern Belgium. *Geomorphology* 337,
486 107582.

487 Bertran P., Andrieux E., Antoine P., Coutard S., Deschodt L., Gardère P., Hernandez M., Legentil C., Lenoble
488 A., Liard M., Mercier N., Moine O., Sitzia L., Van Vliet-Lanoë B., 2014. Distribution and chronology of
489 Pleistocene permafrost features in France: database and first results. *Boreas* 43: 699–711.

490 Bertran P., Bosq M., Borderie Q., Coussot C., Coutard S., Deschodt L., Franc O., Gardère P., Liard M.,
491 Wuscher P., 2021. Revised map of European aeolian deposits derived from soil texture data.
492 *Quaternary Science Reviews* 266, 107085.

493 Bosq M., Bertran P., Degeai J.P., Kreutzer S., Queffelec A., Moine O., Morin E., 2018. Last Glacial aeolian
494 landforms and deposits in the Rhône Valley (SE France): spatial distribution and grain-size
495 characterization. *Geomorphology* 318, 250-269.

496 Brandon A., Sumbler M.G., 1991. The Balderton Sand and Gravel: pre-Weichselian cold stage fluvial
497 deposits near Lincoln, England. *Journal of Quaternary Science* 6 (2), 117-138.

498 Burn C.R., O'Neill H.B., 2015. Subdivision of ice-wedge polygons, western Arctic coast. 7th Canadian
499 Permafrost Conference, Québec, Vol. 1 (<https://www.researchgate.net/publication/282185973>).

500

- 501 Buylaert J.P., Ghysels G., Murray A.S., Thomsen K.J., Vandenberghe D., De Corte F., Heyse I., Van den
 502 Haute P., 2009. Optical dating of relict sand wedges and composite-wedge pseudomorphs in Flanders,
 503 Belgium. *Boreas* 38, 160-175.
- 504 Christensen L., 1974. Crop-marks revealing large-scale patterned ground structures in cultivated areas,
 505 southwestern Jutland, Denmark. *Boreas* 3, 153-180.
- 506 Deschodt L., Munaut A.V., Limondin-Lozouet N., Boulen M. 2008. Lambersart « Les Conquérants »
 507 (vallée de la Deûle, nord de la France) : une transition versant-fond de vallée au début glaciaire et
 508 pléni-glaciaire weichselien. *Quaternaire* 14, 309-333.
- 509 Ehlers J, Gibbard PL., 2004. Quaternary Glaciations-Extent and Chronology, Part I: Europe.
 510 *Developments in Quaternary Science*. Elsevier: Amsterdam; vol. 2a.
- 511 Evans D.J.A., Bateman M.D., Roberts D.H., Medialdea A., Hayes L., Duller G.A.T., Fabel D., Clark C.D.,
 512 2018a. Glacial Lake Pickering: stratigraphy and chronology of a proglacial lake dammed by the North
 513 Sea Lobe of the British–Irish Ice Sheet. *Journal of Quaternary Science* 32 (2), 295-310.
- 514 Evans D.J.A., Roberts D.H., Bateman M.D., Medialdea A., Ely J., Moreton S.G., Clark C.D., Fabel D.,
 515 2018b. Sedimentation during Marine Isotope Stage 3 at the eastern margins of the Glacial Lake Humber
 516 basin, England. *Journal of Quaternary Science* 33 (8), 971-891.
- 517 Evans D.J.A., Roberts D.H., Bateman M.D., Clark C.D., Medialdea A., Callard L., Grimoldi E., Chiverrell
 518 R.C., Ely J., Dove D., Ó Cofaigh C., Saher M., Bradwell T., Moreton S.G., Fabel D., Bradley S.L., 2021.
 519 Retreat dynamics of the eastern sector of the British–Irish Ice Sheet during the last glaciation. *Journal*
 520 *of Quaternary Science* 36, 723-751.
- 521 Ewertowski M., 2009. Ice-wedge pseudomorphs and frost-cracking structures in Weichselian
 522 sediments, central-west Poland. *Permafrost and Periglacial processes* 20, 316-330.
- 523 Ewertowski M.W., Kijowski A., Szuman I., Tomczyk A.M., Kasprzak L., 2017. Low-altitude remote
 524 sensing and GIS-based analysis of cropmarks: classification of past thermal-contraction-crack polygons
 525 in central western Poland. *Geomorphology* 293, 418-432.
- 526 Fábíán S.A., Kovács J., Varga G., Sipos G., Horváth Z., Thamó-Bozsó E., Tóth G., 2014. Distribution of
 527 relict permafrost features in the Pannonian Basin, Hungary. *Boreas* 43, 722–732.
- 528 Fairburn W.A., Bateman M.D., 2016. A new multi-stage recession model for Proglacial Lake Humber
 529 during the retreat of the last British–Irish Ice Sheet. *Boreas* 45, 133-151.
- 530 Fortier D., Allard M., 2005. Frost-cracking conditions, Bylot Island, eastern Canadian Arctic archipelago.
 531 *Permafrost and Periglacial Processes* 16 (2), 145–161.
- 532 Frechen M., Van Vliet-Lanoë B., Van den Haute P., 2001. The Upper Pleistocene loess record at
 533 Harmignies/Belgium – High-resolution terrestrial archive of climate forcing: Palaeogeography,
 534 Palaeoclimatology, Palaeoecology 173, 175-195.
- 535 Gemmell A.M.D., Ralston I.B.M., 1965. Some recent discoveries of ice-wedge cast networks in north-
 536 east Scotland. *Scottish Journal of Geology* 20 (1), 115-118.
- 537 Ghysels G., Heyse I., 2006. Composite-wedge pseudomorphs in Flanders, Belgium. *Permafrost and*
 538 *Periglacial Processes* 17, 145-161.

- 539 Gozdzik J.S., 1986. Structures de fentes à remplissage primaire sableux du Vistulien en Pologne et leur
540 importance paléogéographique. *Biuletyn Peryglacjalny* 31, 71-105.
- 541 Grube A., 2021. Reply to “Discussion on ‘Palaeoseismic structures in Quaternary sediments, related to
542 an assumed fault zone north of the Permian Peissen-Gnutz Salt Structure (NW Germany) – Neotectonic
543 activity and earthquakes from the Saalian to the Holocene’ (Grube, 2019)” by Pascal Bertran, Kevin
544 Manchuel and Deborah Sicilia. *Geomorphology* 385, 107705.
- 545 Hassenpflug W., 2013. Zu Verbreitung und Erscheinungsformen von Polygonmustern in Schleswig-
546 Holstein – eine luftbildgestützte Erfassung. *Natur- und Landeskunde* 120, 49–67.
- 547 Haesaerts P., Van Vliet-Lanoë B., 1973. Evolution d’un permafrost fossile dans les limons du dernier
548 glaciaire à Harmignies (Belgique). *Bulletin de l’Association Française pour l’Etude du Quaternaire* 10
549 (3), 151-164.
- 550 Haltigin T.W., Pollard W.H., Dutilleul P., Osinski G.R., 2012. Geometric evolution of polygonal terrain
551 networks in the Canadian High Arctic: Evidence of increasing regularity over time. *Permafrost and*
552 *Periglacial Processes* 23, 178-186.
- 553 Hammer Ø., Harper D.A.T., Ryan P.D., 2001, PAST. Paleontological Statistics Software package for
554 education and data analysis. *Palaeontologia Electronica* 4, 9.
- 555 Heyse I., Ghysels G., 2003. Fossil polygonal periglacial structures in Flanders (Belgium). *Proceedings of*
556 *the 8th International Conference on Permafrost, Zurich, Switzerland*. Balkema: Lisse; 395–400.
- 557 Hughes A.L.C., Gyllencreutz R., Lohne Ø.S., Mangerud J., Svendsen J.I., 2016. The last Eurasian ice
558 sheets – a chronological database and time-slice reconstruction, DATED-1. *Boreas* 45, 1–45.
- 559 Isarin R, Huijzer B, van Huissteden K. 1998. Time-slice oriented multiproxy database (MPDB) for
560 palaeoclimatic reconstruction. National Snow and Ice Data Center, University of Boulder, Colorado.
561 <http://nsidc.org/data/ggd248.html>
- 562 Janská V., Jiménez-Alfaro B., Chytrý M., Divíšek J., Anenkhnov O., Korolyuk A., Lashchinskyi N., Culek
563 M., 2017. Palaeodistribution modelling of European vegetation types at the Last Glacial Maximum
564 using modern analogues from Siberia: Prospects and limitations. *Quaternary Science Reviews* 159,
565 103-115.
- 566 Jary Z., 2009. Periglacial markers within the Late Pleistocene loess–palaeosol sequences in Poland
567 and Western Ukraine. *Quaternary International* 198, 124-135.
- 568 Johnsson G., 1984. Ice-wedge polygons and other periglacial phenomena in intermorainic sediments
569 in the Öresund area, southern Sweden. *Geologiska Föreningens i Stockholm Förhandlingar* 105 (4),
570 341-348.
- 571 Kasse C., 2002. Sandy aeolian deposits and environments and their relation to climate during the Last
572 Glacial Maximum and Lateglacial in northwest and central Europe. *Progress in Physical Geography* 26
573 (4), 507-532.
- 574 Kjaer K.H., Lagerlun E., Adrielsson L., Thomas P.J., Murray A., Sandgre, P., 2006. The first independent
575 chronology of Middle and Late Weichselian sediments from southern Sweden and the island of
576 Bornholm. *GFF* 128, 209–220.

- 577 Kokelj S.V., Lantz T.C., Wolfe S.A., Kanigan J.C., Morse P.D., Coutts R., Molina-Giraldo N., Burn C.R.,
578 2014. Distribution and activity of ice wedges across the forest-tundra transition, western Arctic
579 Canada. *Journal of Geophysical Research: Earth Surface* 119, 2032-2047.
- 580 Kolstrup E., 1986. Reappraisal of the upper Weichselian Periglacial environment from Danish frost
581 wedge casts. *Palaeogeography, Palaeoclimatology, Palaeoecology* 56, 237-249.
- 582 Kolstrup E., 2004. Stratigraphic and environmental implications of a large ice-wedge cast at Tjaereborg,
583 Denmark. *Permafrost and Periglacial Processes* 15, 31–40.
- 584 Kovács J., Fábrián S.A., Schweitzer F., Varga G., 2007. A Relict Sand-wedge Polygon Site in North-central
585 Hungary. *Permafrost and Periglacial Processes* 18, 379-384.
- 586 Lachenbruch A.H., 1962. Mechanics of the thermal contraction cracks and ice-wedge polygons in
587 permafrost. *Geological Society of America Special Paper* 70.
- 588 Lachenbruch A.H., 1966. Contraction theory of ice-wedge polygons; a qualitative discussion. In
589 *Proceedings, First International Permafrost Conference. National Academy of Science, National*
590 *Research Council of Canada, Publication 1287, 63-71.*
- 591 Lautridou J.P., Sommé J., 1981. L'extension des niveaux-repères périglaciaires à grandes fentes de gel
592 de la stratigraphie du Pléistocène récent dans la France du nord-ouest. *Biuletyn Peryglacjalny* 28, 179-
593 184.
- 594 Lehmkuhl F., Nett J.J., Pötter S., Schulte P., Sprafke T., Jary Z., Antoine P., Wacha L., Wolf D., Zerboni
595 A., Hošek J., Marković S.B., Obreht I., Sümegi P., Veres D., Zeeden C., Boemke B., Schaubert V.,
596 Viehweger J., Hambach U., 2021. Loess landscapes of Europe – Mapping, geomorphology, and zonal
597 differentiation. *Earth-Science Reviews* 215, 103496.
- 598 Mackay J.R., 1975. The closing of ice-wedge cracks in permafrost, Garry Island, Northwest Territories.
599 *Canadian Journal of Earth Sciences* 12, 1668-1674.
- 600 Mackay J.R., Burn C.R., 2002. The first 20 years (1978-1979 to 1998-1999) of ice-wedge growth at the
601 Illisarvik experimental drained lake site, western Arctic coast, Canada. *Canadian Journal of Earth*
602 *Science* 39 (12), 95-111.
- 603 Maddy D., Lewis S.G., Scaife R.G., Bowen D.Q., Coope G.R., Green C.P., Hardaker D., Keen D.H., Rees-
604 Jones J., Parfitt S., Scott K., 1998. The Upper Pleistocene deposits at Cassington, near Oxford, England.
605 *Journal of Quaternary Science* 13 (3), 205-231.
- 606 Magyari E.K., Kuneš P., Jakab G., Sümegi P., Pelánková B., Schäbitz F., Braun M., Chytrý M., 2014. Late
607 Pleniglacial vegetation in eastern-central Europe: are there modern analogues in Siberia? *Quaternary*
608 *Science Reviews* 95, 60-79.
- 609 Mangold N., 2005. High latitude patterned grounds on Mars: Classification, distribution and climatic
610 control. *Icarus* 174, 336-359.
- 611 Matsuoka N., Christiansen H.H., Watanabe T., 2018. Ice-wedge polygon dynamics in Svalbard: Lessons
612 from a decade of automated multi-sensor monitoring. *Permafrost and Periglacial Processes* 29, 210-
613 227.

- 614 Meszner S., Kreutzer S., Fuchs M., Faust D., 2013. Late Pleistocene landscape dynamics in Saxony,
615 Germany: paleoenvironmental reconstruction using loess-paleosol sequences. *Quaternary*
616 *International* 296, 94–107.
- 617 Michel J.P., 1969. Divers types de phénomènes périglaciaires et leur répartition dans les alluvions
618 quaternaires de la Seine et de ses affluents. *Bulletin de l'Association Française pour l'Etude du*
619 *Quaternaire Suppl. 2*, 721–735.
- 620 Michel J.P., 1975. Périglaciaires des environs de Paris. *Biuletyn Peryglacjalny* 24, 259–352.
- 621 Murton J.B., 2013. Ice wedges and ice wedge casts. In: Elias, S.A., Mock, C.J. (Eds.), *Encyclopedia of*
622 *Quaternary Science*. Elsevier, Amsterdam, pp. 436–451.
- 623 Murton J.B., Bowen D.Q., Candy I., Catt J.A., Carrant A., Evans J.G., Frogley M.R., Green C.P., Keen D.H.,
624 Kerney M.P., Parish D., Penkman K., Schreve D.C., Taylor S., Toms P.S., Worsley P., York L.L., 2015.
625 Middle and Late Pleistocene environmental history of the Marsworth area, south-central England.
626 *Proceedings of the Geologists' Association* 126, 18-49.
- 627 Plug L.J., Werner B.T., 2001. Fracture networks in frozen ground. *Journal of Geophysical Research* 106
628 (B5), 8599-8613.
- 629 Plug L.J., Werner B.T., 2002. Nonlinear dynamics of ice-wedge networks and resulting sensitivity to
630 severe cooling events. *Nature* 417, 929-932.
- 631 Plug L.J., Werner B.T., 2008. Modelling of ice-wedge networks. *Permafrost and Periglacial Processes*
632 19, 63-69.
- 633 Ruzkiczay-Rüdiger Z., Kern Z., 2016. Permafrost or seasonal frost? A review of paleoclimate proxies of
634 the last glacial cycle in the East Central European lowlands. *Quaternary International* 415, 241-252.
- 635 Schmidt C., Zeeden C., Krauss L., Lehmkuhl F., Zöller L., 2021. A chronological and palaeoenvironmental
636 re-evaluation of two loess-palaeosol records in the northern Harz foreland, Germany, based on
637 innovative modelling tools. *Boreas* 50, 746-753.
- 638 Seddon M.B., Holyoak D.T., 1985. Evidence of sustained regional permafrost during deposition of
639 fossiliferous Late Pleistocene river sediments at Stanton Harcourt (Oxfordshire, England). *Proceedings*
640 *of the Geologists' Association* 96 (1), 53-71.
- 641 Sitzia L., Bertran P., Bahain J.J., Bateman M.D., Hernandez M., Garon H., De Lafontaine G., Mercier N.,
642 Leroyer C., Queffelec A., Voinchet P., 2015. The quaternary coversands of southwest France.
643 *Quaternary Science Reviews* 124, 84–105.
- 644 Sletten R.S., Hallet B., Fletcher R.C., 2003. Resurfacing time of terrestrial surfaces by the formation and
645 maturation of polygonal patterned ground. *Journal of Geophysical Research* 108, E4, 8044.
- 646 Stadelmaier K.H., Ludwig P., Bertran P., Antoine P., Shi X., Lohmann G., Pinto J.G., 2021. A new
647 perspective of permafrost boundaries in France during the Last Glacial Maximum. *Climate of the Past*,
648 <https://doi.org/10.5194/cp-2021-60>.
- 649 Strandberg G., Brandefelt J., Kjellström E., Smith B., 2011. High-resolution regional simulation of last
650 glacial maximum climate in Europe. *Tellus A: Dynamic Meteorology and Oceanography* 63, 107–125.

- 651 Svensson H., 1973. Distribution and chronology of relict polygon patterns on the Laholm plain, the
652 Swedish coast. *Geografiska Annaler* 54A, 3-4, 159-175.
- 653 Svensson H., 1988. Ice-wedge casts and relict polygonal patterns in Scandinavia. *Journal of Quaternary*
654 *Science* 3 (1), 57-67.
- 655 Ulrich M., Hauber E., Herzs Schuh U., Härtel S., Schirrmeister L., 2011. Polygon pattern geomorphometry
656 on Svalbard (Norway) and western Utopia Planitia (Mars) using high-resolution stereo remote-sensing
657 data. *Geomorphology* 134, 197-216.
- 658 Vandenberghe J., Krook L., 1981. Stratigraphy and genesis of Pleistocene deposits at Alphen (southern
659 Netherlands). *Geologie en Mijnbouw* 60, 417-426.
- 660 Vandenberghe J, French H, Gorbunov A, Marchenko S, Velichko AA, Jin H, Cui Z, Zhang T, Wan X. 2014.
661 The Last permafrost Maximum (LPM) map of the Northern Hemisphere: permafrost extent and mean
662 annual air temperatures, 25-17 ka. *Boreas* 43, 652-666.
- 663 Watson E., 1965. Periglacial structures in the Aberystwyth region of central Wales. *Proceedings of the*
664 *Geologists' Association* 76 (4), 443-462.
- 665 Williams R.B.G., 1964. Fossil patterned ground in eastern England. *Biuletyn Peryglacjalny* 22, 337-349.
- 666 Wolfe S. A., Morse P. D., Neudorf C. M., Kokelj S. V., Lian O. B., O'Neill H. B., 2018. Contemporary sand
667 wedge development in seasonally frozen ground and paleoenvironmental implications,
668 *Geomorphology* 308, 215 - 229.
- 669 Worsley P., 2014. Ice-wedge growth and casting in a Late Pleistocene, periglacial, fluvial succession at
670 Baston, Lincolnshire. *Mercian Geologist* 18 (3), 159-170.
- 671 Zeeberg J., 1998. The European sand belt in Eastern Europe - and comparison of Late Glacial dune
672 orientation with GCM simulation results. *Boreas* 27, 127-139.

673

674 **Figure captions**

675 Figure 1: Types of crack junctions. A – initial cracks; B – after substantial wedge growth.

676 Figure 2: Distribution map of polygons in Europe. Ice sheet limits are from [Hugues et al. \(2016\)](#) for the
677 Fennoscandian Ice Sheet (FIS) and British-Irish Ice Sheet (BIIS) and from [Ehlers and Gibbard \(2004\)](#) for
678 the other ice sheets. The map of aeolian deposits is from [Bertran et al. \(2021\)](#). AU: Austria, BE: Belgium,
679 CZ: Czech Republic, DK: Denmark, FR: France, GE: Germany, HU: Hungary, IT: Italy, NE: Netherlands,
680 PO: Poland, SP: Spain, SW: Sweden.

681 Figure 3: Association between the distribution of polygons and aeolian sand sources in mid-latitudes.
682 A - Loire Valley (France), the map of aeolian deposits from [Bertran et al. \(2021\)](#) is superimposed on a
683 simplified 1:250,000 geological map; B - Main Valley, Central Germany on 1:200,000 geological map
684 background (<https://services.bgr.de/wms/geologie/guek200/>).

685 Figure 4: Number of polygons identified according to lithology.

686 Figure 5: Size of the polygons. A - Size according to lithology, whole dataset; B - Size according to
687 sediment age, selected areas from northern Europe; C – Size according to latitude, whole dataset.

688 Figure 6: Size of polygons as a function of age. A - Denmark and southern Sweden, ice sheet limits are
689 from [Hughes et al. \(2016\)](#) except for the boundary at 17 ka (2), which is from [Evans et al. \(2021\)](#); B –
690 UK, the map of the Fenland, Humber, and Pickering proglacial lakes is from [Fairburn and Bateman](#)
691 [\(2016\)](#).

692 Figure 7: Types of polygons. A - Regular hexagonal polygons, Chevrolières_3, France; B - Irregular
693 mixed polygons, Dimbach_2, Germany; C - Orthogonal polygons (top of the picture) juxtaposed to
694 hexagonal polygons (bottom), Isengerode, Germany; D - Regular orthogonal polygons, Bielawy,
695 Poland; E- Subdivided orthogonal polygons, Dziewa, Poland; F - Oriented orthogonal polygons,
696 Bedford, UK.

697 Figure 8: Types of polygons, whole dataset. A - Regularity as a function of type; B - Types as a
698 function of lithology; C - Size as a function of regularity; D - Types as a function of latitude; E -
699 Regularity as a function of latitude.

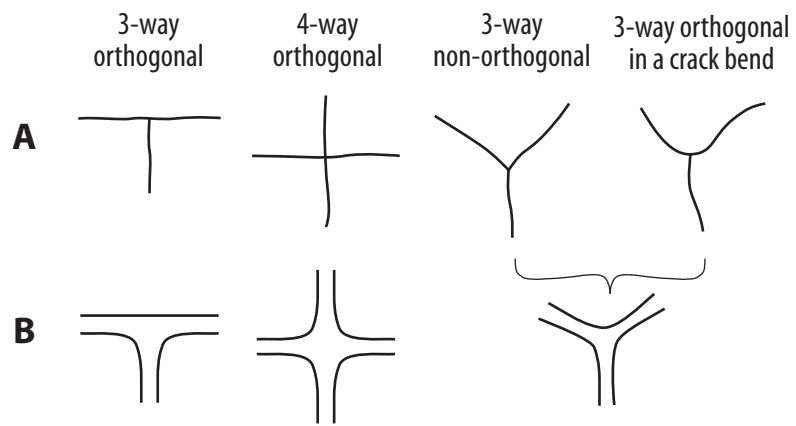
700 Figure 9: Difference in altitude (Δalt) between polygons and surrounding terrain (1 km buffer).
701 Negative values indicate that the polygons were formed in a depression.

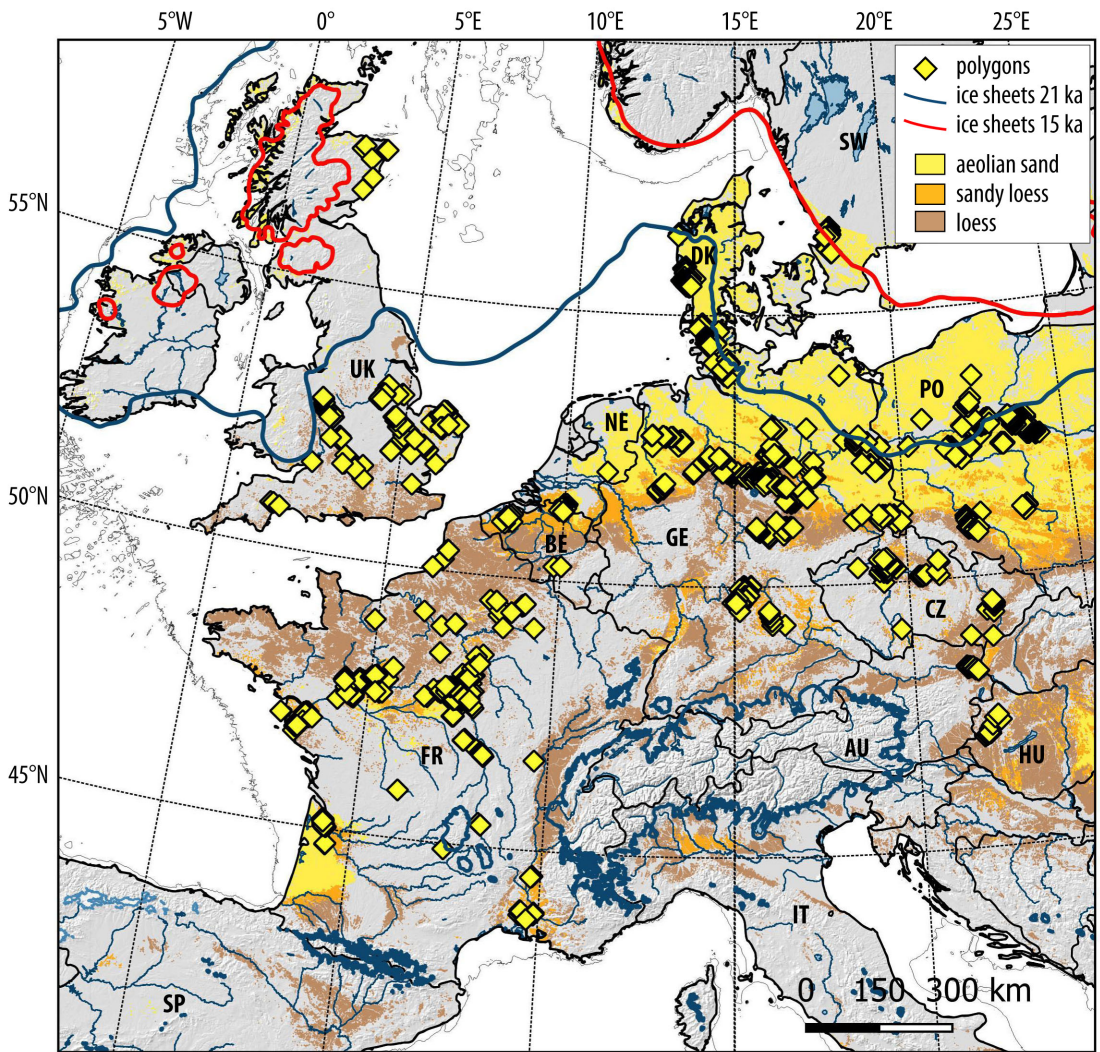
702 Figure 10: Irregular young polygons. A - Skogaby, Sweden (deglaciation < 15 ka); B - Össjö_3, Sweden
703 (deglaciation < 17 ka); C – Grabionna, Poland (deglaciation < 19 ka); D – Friedersdorf_2, Germany
704 (deglaciation < 21 ka).

705 Figure 11: Subdivided polygons. A - Great Milton, UK; B - Gerholzhofen, Germany.

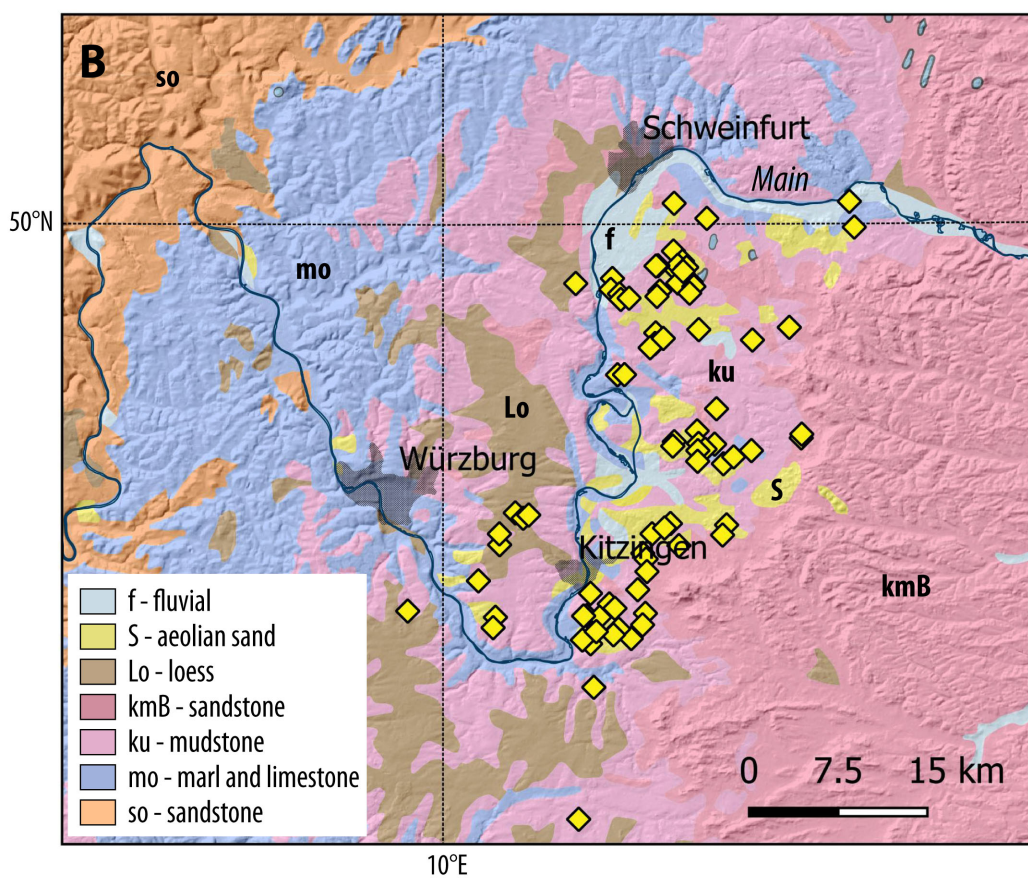
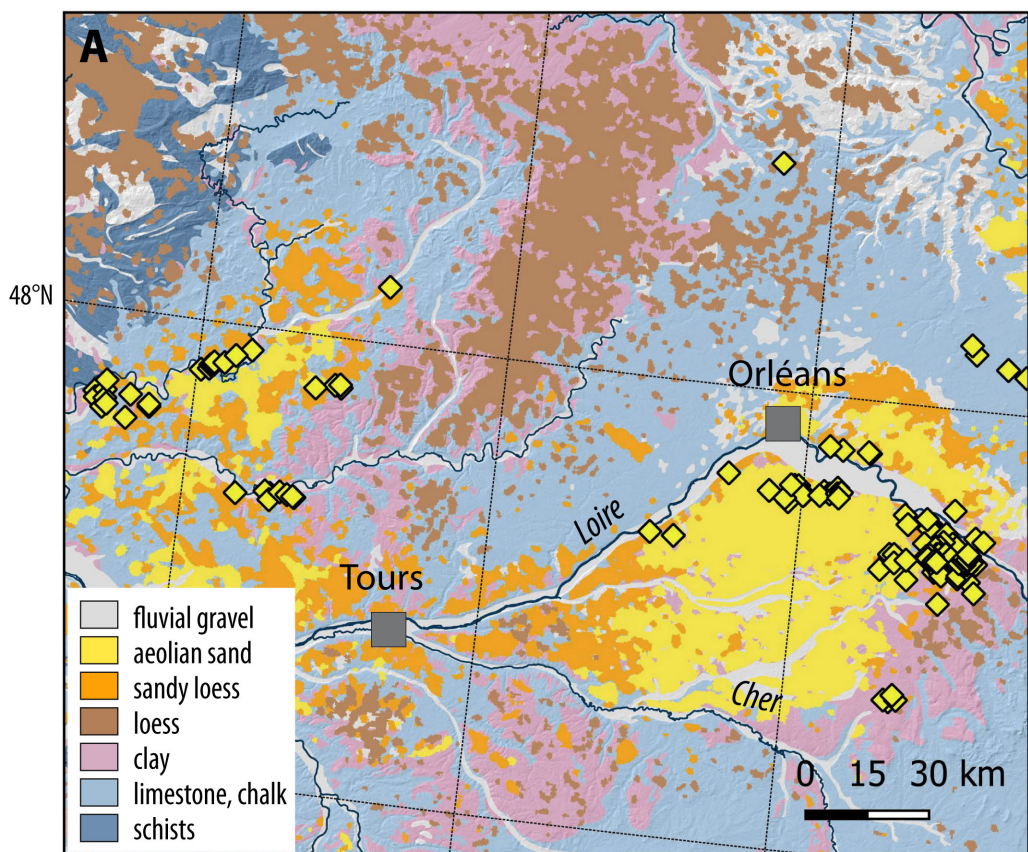
706 Figure 12: Proportion of 4-way junctions as a function of polygon age (A) and lithology (B).

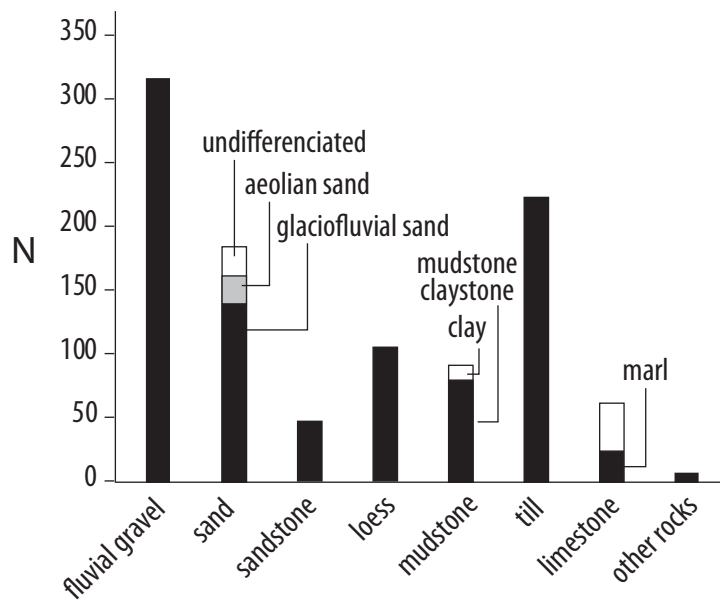
707 Figure 13: Distribution of Pleistocene (mostly Weichselian) ice-wedge pseudomorphs, composite
708 wedge pseudomorphs and relict sand wedges, after [Isarin et al. \(1998\)](#), [Andrieux et al. \(2016a\)](#) and
709 this study. The limits of continuous permafrost and discontinuous to sporadic permafrost at 21 ka are
710 from [Stadelmeier et al. \(2021\)](#).

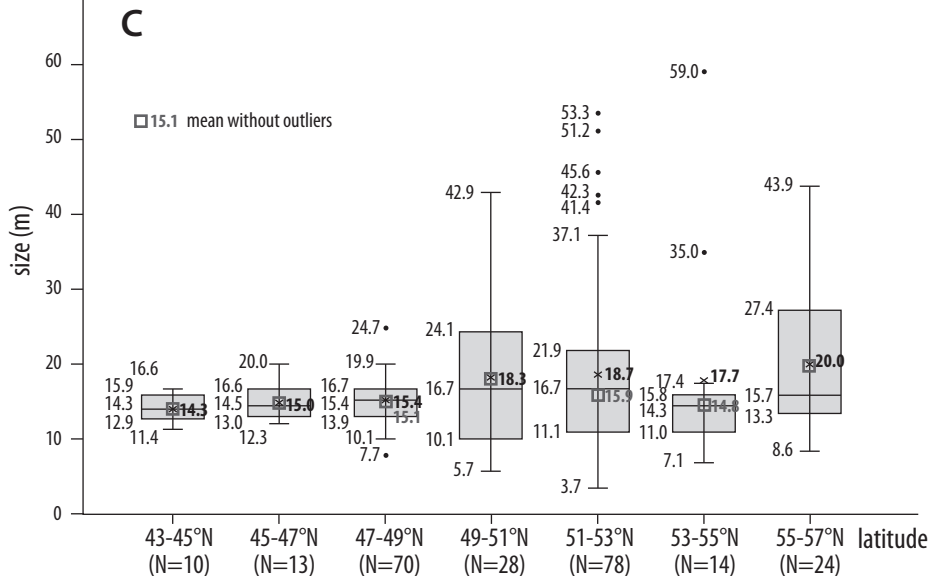
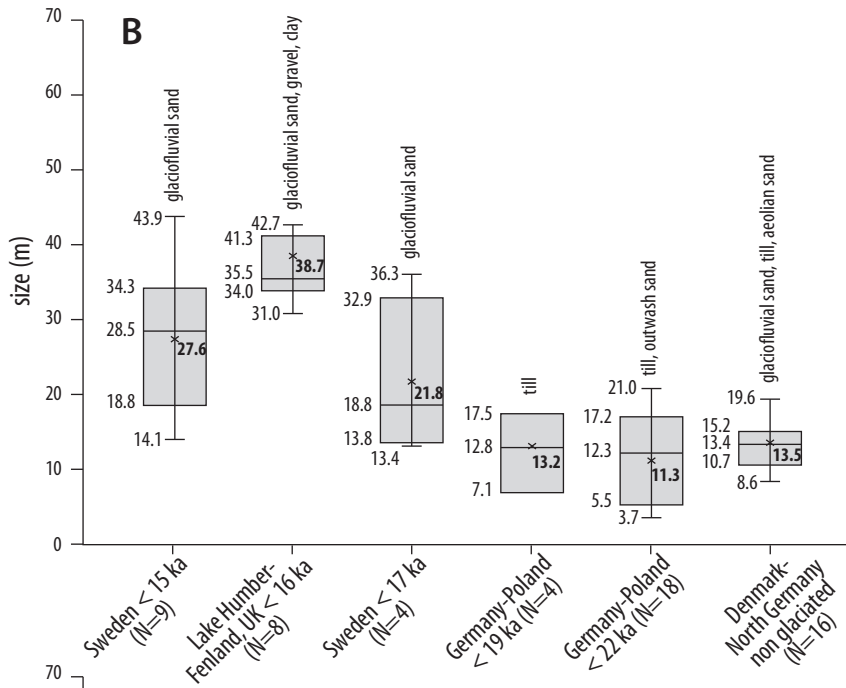
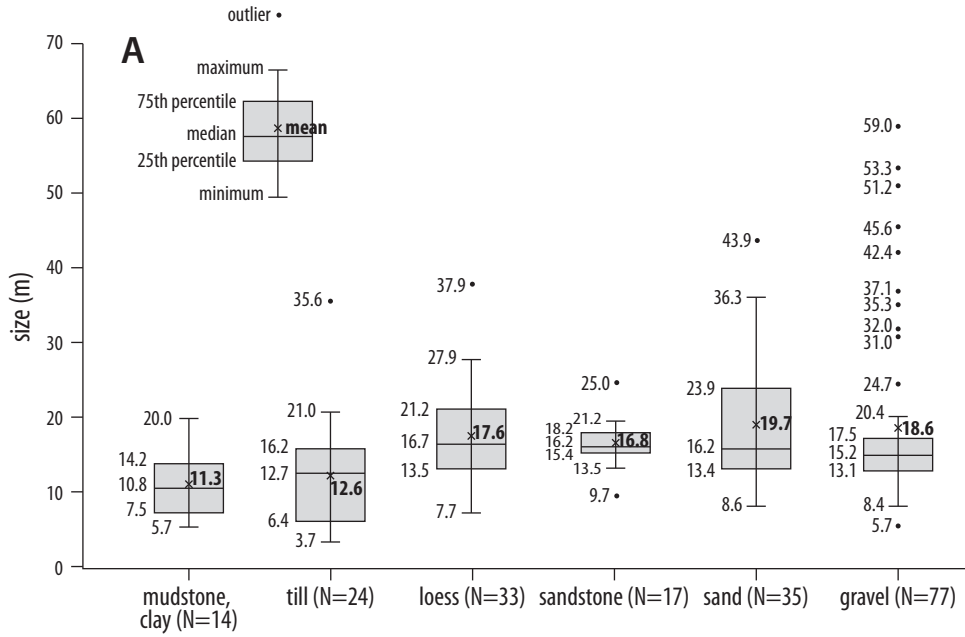




0° 1°E 2°E

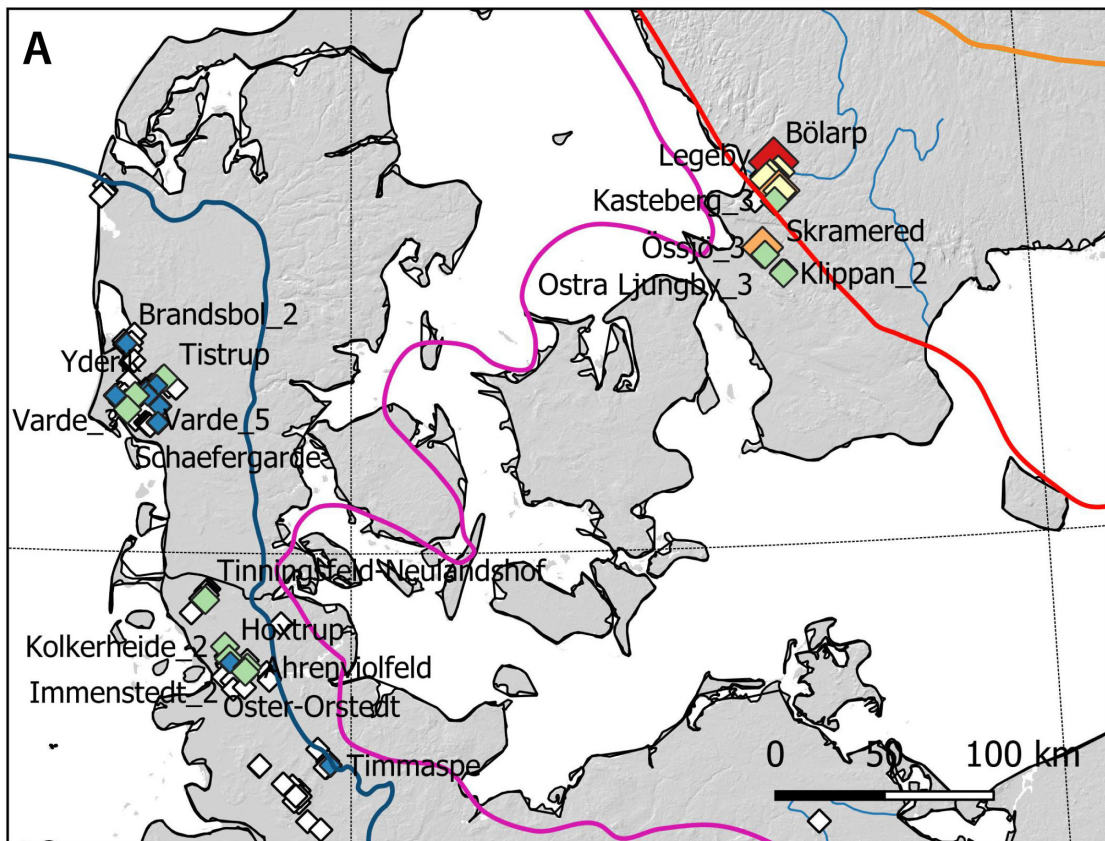




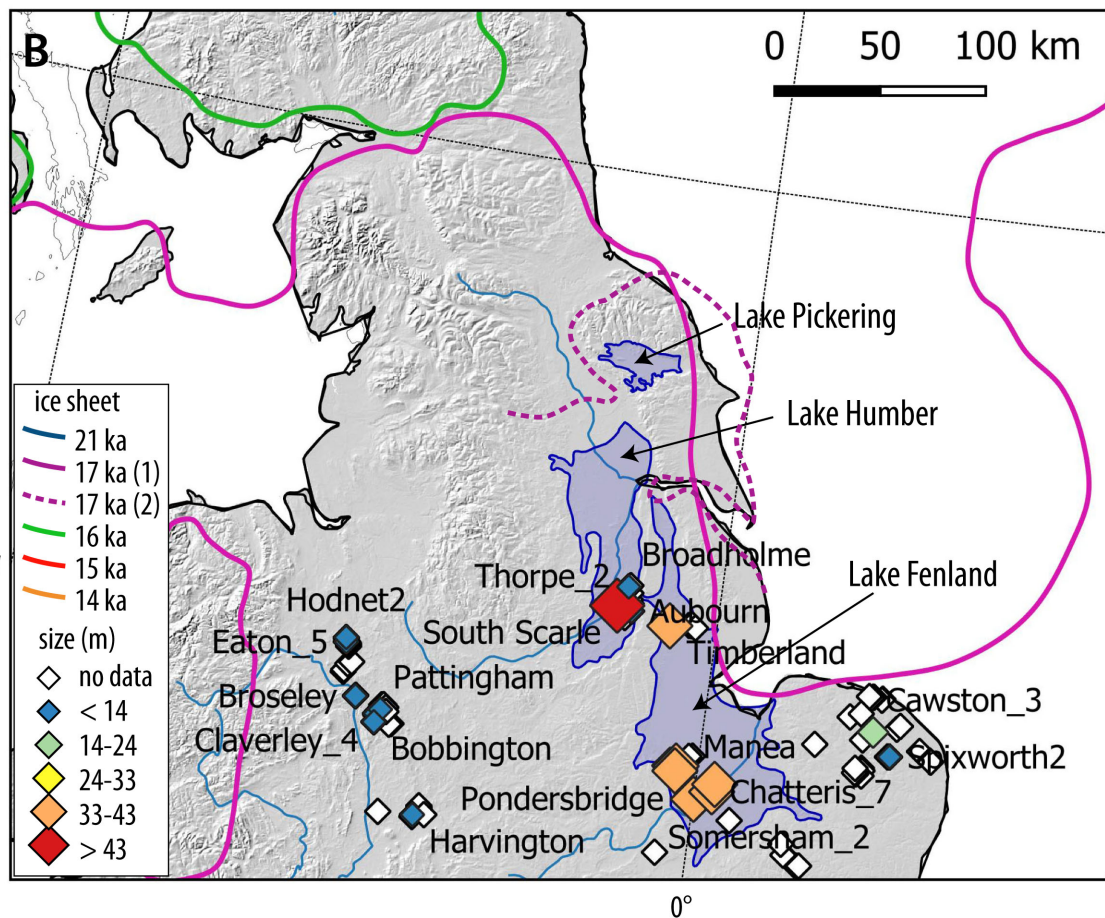


10°E

15°E



55°N



0

50

100 km

0°

